Entropy-Driven Enhanced Self-Diffusion in Confined Reentrant Supernematics

Marco G. Mazza,[1] Manuel Greschek,[1] Rustem Valiullin,[2] Jörg Kärger,[2] and Martin Schoen[1,3]

[1]*Stranski-Laboratorium für Physikalische und Theoretische Chemie, Technische Universität Berlin, Straße des 17. Juni 135, 10623 Berlin, Germany*

[2]*Institut für Experimentelle Physik I, Universität Leipzig, Linnéstraße 5, 04103 Leipzig, Germany*

[3]*Department of Chemical and Biomolecular Engineering, North Carolina State University, 911 Partners Way, Raleigh, North Carolina 27695, USA*

(Received 10 May 2010; published 24 November 2010)

We present a molecular dynamics study of reentrant nematic phases using the Gay-Berne-Kihara model of a liquid crystal in nanoconfinement. At densities above those characteristic of smectic *A* phases, reentrant nematic phases form that are characterized by a large value of the nematic order parameter $S \simeq 1$. Along the nematic director these ''supernematic'' phases exhibit a remarkably high self-diffusivity, which exceeds that for ordinary, lower-density nematic phases by an order of magnitude. Enhancement of self-diffusivity is attributed to a decrease of rotational configurational entropy in confinement. Recent developments in the pulsed field gradient NMR technique are shown to provide favorable conditions for an experimental confirmation of our simulations.

DOI: 10.1103/PhysRevLett.105.227802 PACS numbers: 61.30.Hn, 61.30.Gd, 64.70.M−, 66.10.C−

In the context of phase transitions, ''reentrancy'' refers to a nonmonotonic variation of an order parameter with the thermodynamic field driving the transition. Reentrancy is ubiquitous in the physics of thermal many-particle systems. It arises under disparate physical conditions, for example, in quantum gases [1], two-dimensional charged colloids [2], or relativistic scalar field models [3]. In soft-matter systems, reentrancy has been reported for self-assembled supramolecular structures [4,5], wetting phenomena at oleophilic surfaces [6], and discotic and calamitic liquid crystals [7]. In fact, since the first observation of reentrant nematic (RN) phases in a seminal paper by Cladis [8], reentrancy in liquid crystals (LC) seems to have received most of the attention. This is most likely because of the abundance of phases exhibited by these materials. For example, reentrant phase transitions have been reported for the isotropic phase of mixtures of discotic LC [9], the ferroelectric transition in syn- and anticlinic smectic *C* phases [10], the cholesteric-to-blue phase transition in chiral LC [11], and nematic (N) phases [12].

Despite the variety of systems and thermodynamic conditions under which reentrancy in LC materials arises, comparatively little attention has been paid to the dynamics of RN phases. For example, distinct differences in the molecular dynamics in the N and RN phases can be concluded from corresponding changes in the nuclear magnetic relaxation times reported in Refs. [13–15].

Whereas most earlier work on reentrancy of phase transitions in LC is experimental in nature, comparatively little attention has been paid to this fascinating phenomenon from a theorist's point of view [16]. The most recent theoretical study employs isothermal-isobaric and canonical ensemble Monte Carlo (MC) simulations to investigate the nature of the smectic *A* (smA)-RN phase transition for a bulk system of hard ellipsoids [17]. Unfortunately, the model employed in Ref. [17] is somewhat artificial in assuming that the ellipsoidal molecules are always oriented perfectly parallel such that all rotational degrees of freedom are always ''frozen'' irrespective of the thermodynamic conditions. Therefore, this study seems only of limited use to elucidate properties of RN phases at a molecular level. Moreover, the authors do not consider dynamic features of RN phases.

Here, we show that the smA-RN phase transition causes a dramatic increase in the self-diffusion of the molecules in the direction of the nematic director $\hat{\boldsymbol{n}}$. Our model system consists of soft spherocylinders interacting via the so-called Gay-Berne-Kihara pair potential [18]; specifically, we use the original version of the model, GBK(6,5,2,1) in the notation of Ref. [18]. Data will be presented for a system of spherocylinders confined to a slit pore with structureless walls, separated by a distance $s_z = 19\sigma$ along the z axis. The fluid-solid interaction is described by the surface-averaged potential [19]

$$u_{\mathrm{fs}} = 4\varepsilon_{\mathrm{fs}}\rho_s\sigma^2\left[\left(\frac{\sigma}{d_w}\right)^{10} - \left(\frac{\sigma}{d_w}\right)^{4} g(\hat{\boldsymbol{u}})\right], \qquad (1)$$

where $\varepsilon_{\mathrm{fs}}$ determines the attractive well depth, $\rho_s\sigma^2 = 2^{-1/3}$ is the areal density of a layer of substrate atoms, d_w is the minimum distance of a spherocylinder from either substrate, and $g(\hat{\boldsymbol{u}})$ is the ''anchoring function,'' where the unit vector $\hat{\boldsymbol{u}}$ specifies the orientation of a molecule [20]. Here, $g(\hat{\boldsymbol{u}}) = u_x^2 + u_y^2$ favors energetically an orientation parallel to the substrate plane [21].

We employ both extensive isothermal-isobaric MC and microcanonical molecular dynamics (MD) simulations to locate the smA-RN phase transition and to study changes in mass transport accompanying that transition.

The main purpose of employing MC calculations is to provide suitably equilibrated starting configurations for subsequent MD simulations. In addition, MC calculations are used to independently verify the correctness of the MD simulations through a comparison of equilibrium properties obtained in both types of simulations. In MC simulations we use a standard algorithm [22] but allow the side lengths of the computational cell to vary independently to preserve the in-plane isotropy of the pressure tensor even in highly ordered confined phases; for more details, see Ref. [23]. We employ the customary dimensionless units of σ for length, ε/k_B for temperature T, and $(\sigma^2 m/\varepsilon)^{1/2}$ for time t, where $m = 1$ is the spherocylinder mass. Values for σ and ε are taken from Ref. [18]. Our simulations comprise $N = 1000$ molecules of length $L = 6$. We truncate interactions beyond a minimum distance $d_m = 3$ and in MD use an integration time step of $\Delta t = 10^{-4}$.

To characterize the degree of nematic order, we compute the nematic order parameter S as the ensemble average of the largest eigenvalue of the instantaneous alignment tensor [24], and its associated eigenvector corresponds to $\hat{\boldsymbol{n}}$. The layering characteristic of smA phases is quantitatively described through the function [20]

$$\lambda(d) \equiv \left\langle \left| \frac{1}{N} \sum_{j=1}^{N} \exp\left[\frac{2\pi i (\mathbf{r}_j \cdot \hat{\boldsymbol{n}})}{d} \right] \right| \right\rangle, \tag{2}$$

where d is the spacing between layers and the smectic order parameter Λ is defined as the maximum of $\lambda(d)$ in the interval $[L - \zeta, L + \zeta]$, where $\zeta = 0.05$. Focusing on $T = 4.0$ first, plots in Fig. 1 show that S is rather small up to a number density $\rho \lesssim 0.09$, indicating that the confined fluid is in its isotropic phase. Beyond $\rho \gtrsim 0.09$, S rises steeply, assuming values characteristic of nematic phases ($S \gtrsim 0.4$) and levels off as ρ increases. At the highest densities considered $S \simeq 1$, which reflects a nearly perfect orientation of molecules. Over the same range of densities, Λ is very small up to values of $\rho \simeq 0.115$, indicating that the confined fluid does not form any smectic layers. As the density increases further, smectic layers are forming revealed by $\Lambda \gtrsim 0.5$. Interestingly, as the density keeps increasing beyond $\rho \simeq 0.135$, Λ drops to a low value of about 0.1, whereas S increases further towards its maximum value of about 1. Hence, $\rho \simeq 0.135$ demarcates the formation of a RN phase. The structural characteristics of confined phases pertaining to the stable regime of N, smA, and RN phases is illustrated by "snapshots" of configurations generated in MD (see Fig. 2). Notice the presence of distinct molecular layers in the smA state which disappear once the RN state forms. By comparing snapshots for typical N and RN phases, it is apparent from Fig. 2 that the latter exhibit much more orientational but roughly the same positional order compared with the former.

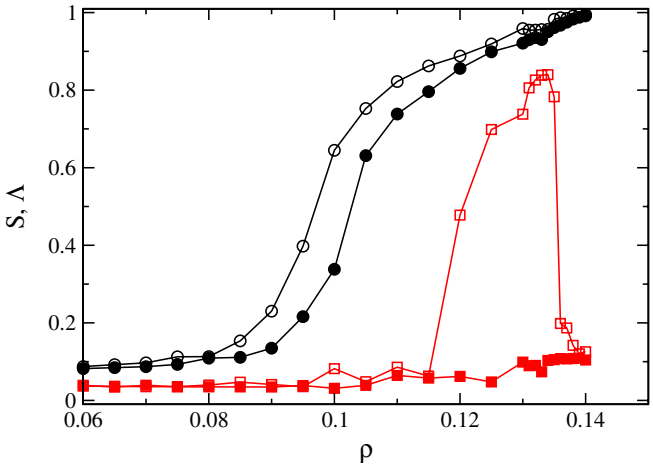

FIG. 1 (color online). Plots of S (○, ●) and Λ (□, ■) as functions of number density ρ for confined LC. Open and filled symbols refer to $T = 4.0$ and 6.0, respectively.

The key result of our study concerns the self-diffusion of molecules in the direction of their orientation. To that end, we introduce the parallel mean-square displacement (MSD)

$$\langle \Delta r_{\parallel}^2(\tau) \rangle_t \equiv \frac{1}{N} \left\langle \sum_{i=1}^{N} \{ \hat{\boldsymbol{u}}_i \cdot [\boldsymbol{r}_i(t+\tau) - \boldsymbol{r}_i(t)] \}^2 \right\rangle_t. \tag{3}$$

The angular brackets indicate an average over the N molecules and time origins referred to by subscript "t". In Fig. 3, we present plots of the MSD for typical N, smA, and RN phases where different time regimes can be identified. In the double-logarithmic representation, short-time slopes of the MSDs exceed their long-time counterparts on account of the initial ballistic motion of molecules in all three phases. As expected, the MSDs are indistinguishable for $\tau \lesssim 0.1$. In the limit of large τ, the time dependence of the MSDs corresponds to diffusive motion; that is, the MSDs depend linearly on τ. The MSD for the smA phase exhibits a plateau at intermediate times which eventually gives way to diffusive motion at long times. The plateau reflects the presence of smectic layers that hinder molecular motion in the direction perpendicular to the plane of adjacent smectic layers (see Fig. 2). In the limit $\tau \to \infty$, reliable values of $D_{\parallel}$ can be extracted from the plots in Fig. 3 via the Einstein relation [25,26]

$$D_{\parallel} = \lim_{\tau \to \infty} \frac{1}{2\tau} \langle \Delta r_{\parallel}^2(\tau) \rangle_t. \tag{4}$$

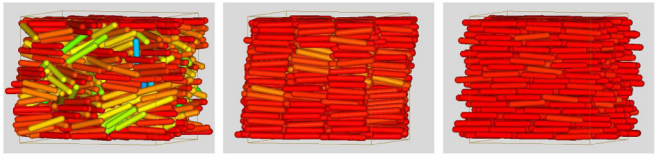

FIG. 2 (color online). Configuration snapshots from MD; $\rho = 0.110$ (left, N), 0.133 (middle, smA), and 0.139 (right, RN), and $T = 4.0$. Color code: $\hat{\boldsymbol{u}}_i \cdot \hat{\boldsymbol{n}} = 0$, blue (light gray); $\hat{\boldsymbol{u}}_i \cdot \hat{\boldsymbol{n}} = 1$, red (dark gray), $i = 1, \ldots, N$.

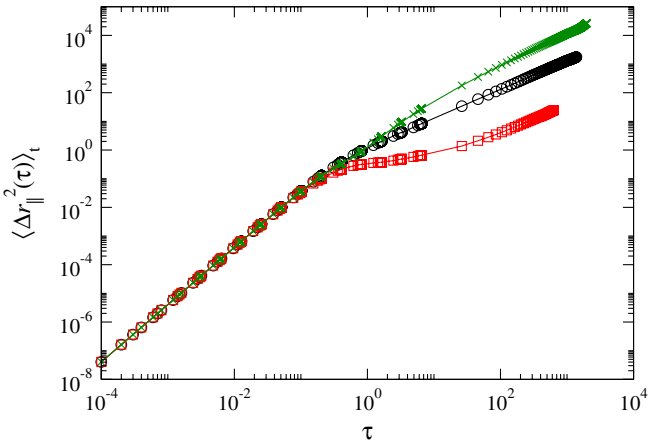

FIG. 3 (color online). MSDs in the confined N (○, $\rho = 0.110$), smA (□, $\rho = 0.133$), and RN phases (×, $\rho = 0.139$) at $T = 4.0$.

A comparison of plots in Figs. 1 and 4 reveals that, in the N phase, $D_\parallel$ is small but nonzero. It attains a nearly vanishing value in the smectic phase on account of layer formation (see Fig. 2), which blocks mass transport efficiently in the direction of the layer normal [25]. Most importantly, however, compared with the smA phases, $D_\parallel$ increases dramatically by several orders of magnitude when the RN phases become thermodynamically stable (i.e., for $\rho \gtrsim 0.135$; see the inset in Fig. 4). Because of the unusually large $D_\parallel$ in conjunction with high nematic order ($S \simeq 1$; see Fig. 1), we call these high-density nematic phases supernematic. One also notices by comparing data for different T in Fig. 4 that both data sets show a similar large increase of $D_\parallel$ beyond a certain density threshold. However, the plot for $T = 6.0$ exhibits nonzero values of $D_\parallel$ over a density range where the corresponding curve for the lower $T = 4.0$ drops to zero. This is due to the absence of smA phases at $T = 6.0$ (see Fig. 1). Interestingly, the experimentally determined phase diagram presented by Guillon, Cladis, and Stamatoff also suggests the absence of intermittent smA phases and a continuous transition from N to RN phases under suitable thermodynamic conditions [27]. Nevertheless, the increase in orientational order for $\rho \gtrsim 0.135$ and $T = 6.0$ causes $D_\parallel$ to increase equally strongly. Hence, at sufficiently high T one may observe supernematic features *without* reentrancy.

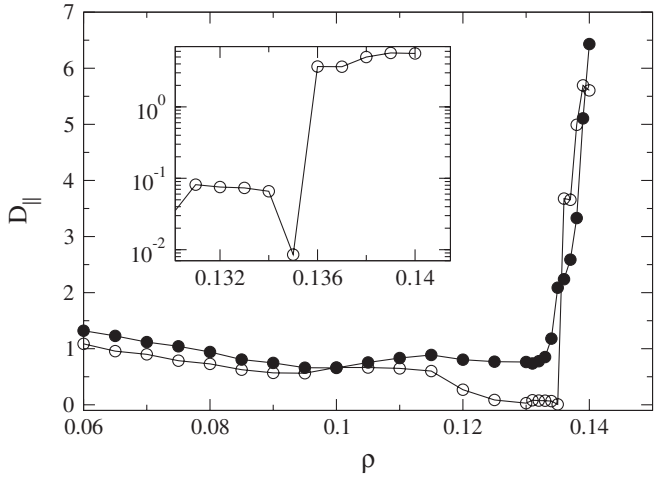

FIG. 4. $D_\parallel$ [see Eq. (4)] as a function of ρ for the confined LC; (○) $T = 4.0$, (●) $T = 6.0$. The inset is a magnification of the $T = 4.0$ isotherm around the smA-RN transition.

The dramatic increase of $D_\parallel$ in the RN phase can be attributed to a loss of rotational configurational entropy $\mathcal{S}_{\rm rc}$ due to both an increase in density and the presence of solid surfaces. We rationalize this by assuming a characteristic time interval $\tau_\parallel$ associated with the onset of diffusive motion in the direction of $\hat{\boldsymbol{n}}$ such that $D_\parallel \propto 1/\tau_\parallel$. For $\tau \geq \tau_\parallel$ the probability $\mathcal{P}$ that a molecule has traveled a distance $\Delta r_\parallel$ from its origin at $\tau = 0$ in the direction of $\hat{\boldsymbol{n}}$ should then also be inversely proportional to $\tau_\parallel$. Intuitively, one expects $\mathcal{P}(\Delta r_\parallel)$ to be larger if the alignment of molecules with $\hat{\boldsymbol{n}}$ is more pronounced on average, that is, the larger S is. However, a larger value of S implies a lower rotational configurational entropy $\mathcal{S}_{\rm rc}$ such that $\mathcal{P} \propto \exp(-\mathcal{S}_{\rm rc}/k_B)$ by using standard statistical-physical reasoning [28]. This then suggests $D_\parallel \propto \exp(-\mathcal{S}_{\rm rc}/k_B)$. We estimate $\mathcal{S}_{\rm rc}$ via

$$\mathcal{S}_{\rm rc} = -k_B \int d\theta P(\theta) \ln P(\theta), \tag{5}$$

where $P(\theta)$ is the distribution of angles $\cos\theta_i = \hat{\boldsymbol{u}}_i \cdot \hat{\boldsymbol{n}}$. By assuming $P(\theta)$ to be Gaussian with a standard deviation of $\sigma_{\rm rc}$, it is easy to verify that $\mathcal{S}_{\rm rc} \propto \ln\sigma_{\rm rc}$. A similar relation was obtained for the configurational entropy of a macromolecule in Ref. [29] by assuming a Gaussian distribution of relevant internal degrees of freedom. Hence, the above line of arguments suggests $D_\parallel \propto \sigma_{\rm rc}^{-1}$, which is supported by plots in Fig. 5.

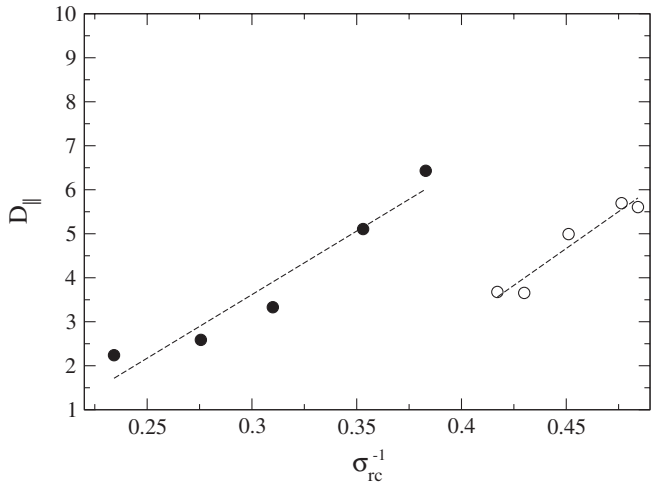

FIG. 5. $D_\parallel$ as a function of $\sigma_{\rm rc}^{-1}$ for $T = 4.0$ (○) and $T = 6.0$ (●). The linear fit (dashed line) is rationalized in the text.

In summary, we have shown for the first time that supernematic LC phases exhibit unusually large self-diffusivity which can be explained in terms of a substantially reduced $\mathcal{S}_{rc}$. Here the suppression of $\mathcal{S}_{rc}$ is assisted by confinement to a nanoscopic slit pore where the solid substrates favor a planar arrangement of the molecules with respect to the substrate plane. Because the solid surfaces of the slit pore may be viewed as the representation of an external field superimposed onto the intermolecular interactions, we anticipate the results presented here to be generic in that they should persist in other fluids composed of anisometric molecules that are exposed to external fields (e.g., dipolar fluids in external magnetic fields). Hence, we believe our results to be important for a broad range of LC applications ranging from lubricants in nanotribology [30] over nanosensors [31] to photonic [32] and organic electronic devices [33] where the mobility of molecules plays a key role.

Though the available experimental data do not yet provide a rigorous confirmation of our theoretical predictions, some of these data are in reasonable qualitative agreement with our simulations. For example, extrapolating longitudinal relaxation rates reported in Ref. [14] from the RN to the N phase yields values markedly below those in the N phase. If referred to the same T, these relaxation rates correspond to correlation times that are notably shorter in the RN compared with the N phase. However, this general interpretation of NMR data remains speculative as long as translational diffusion has not definitely been identified as the process governing the observed relaxation.

Direct evidence for the relation between translational diffusion and NMR data can be provided by the pulsed field gradient NMR (PFG NMR) technique [34], which records molecular displacements typically over a micrometer range. For example, PFG NMR has been applied to directly assess the diffusion tensor upon entering the N phase [35]. There, diffusion in the direction of the molecules' long axes was found to increase with increasing nematic order. Similarly, the diffusivity of n-alkanes in nanochannels was found to increase with increasing orientational order [36]. These findings are in line with our data where enhanced molecular ordering is accompanied by increasing diffusivities in the direction of $\hat{\boldsymbol{n}}$. The powerful combination of PFG NMR with magic angle spinning has recently enabled a notable increase in both observation times and gradient pulse intensities [37]. As a consequence, PFG NMR diffusion measurements became possible beyond the limits of measurability existing so far. This concerns, in particular, the first diffusion measurements with LC confined to nanopores [38]. To stimulate a direct experimental verification of our present predictions using these novel techniques is the primary purpose of this study.

Financial support from the International Graduate Research Training Group 1524-DFG is gratefully acknowledged.

[1] H. Kleinert, S. Schmidt, and A. Pelster, Phys. Rev. Lett. **93**, 160402 (2004).
[2] C. Bechinger *et al.*, J. Phys. Condens. Matter **12**, A425 (2000).
[3] M. B. Pinto, R. O. Ramos, and J. E. Parreira, Phys. Rev. D **71**, 123519 (2005).
[4] N. Osaka *et al.*, J. Chem. Phys. **127**, 094905 (2007).
[5] J. Dudowicz *et al.*, J. Chem. Phys. **130**, 164905 (2009).
[6] S. M. M. Ramos *et al.*, Langmuir **26**, 5141 (2010).
[7] J. Szydlowska *et al.*, J. Mater. Chem. **18**, 1108 (2008).
[8] P. E. Cladis, Phys. Rev. Lett. **35**, 48 (1975).
[9] W. K. Lee *et al.*, Liq. Cryst. **4**, 87 (1989).
[10] D. Pociecha *et al.*, Phys. Rev. Lett. **86**, 3048 (2001).
[11] G. Heppke *et al.*, Liq. Cryst. **8**, 407 (1990).
[12] G. Sigaud *et al.*, Mol. Cryst. Liq. Cryst. **69**, 81 (1981).
[13] R. Y. Dong, J. Chem. Phys. **75**, 2621 (1981); **76**, 5659 (1982).
[14] S. Miyajima *et al.*, Solid State Commun. **49**, 675 (1984).
[15] J. Bharatam and C. R. Bowers, J. Phys. Chem. B **103**, 2510 (1999).
[16] R. R. Netz and A. N. Berker, Phys. Rev. Lett. **68**, 333 (1992).
[17] E. de Miguel and E. Martín del Río, Phys. Rev. Lett. **95**, 217802 (2005).
[18] B. Martínez-Haya *et al.*, J. Chem. Phys. **122**, 024908 (2005).
[19] M. Schoen and S. H. L. Klapp, *Nanoconfined Fluids. Soft Matter between Two and Three Dimensions* (Wiley-VCH, New York, 2007).
[20] H. Steuer, S. Hess, and M. Schoen, Phys. Rev. E **69**, 031708 (2004).
[21] M. Greschek *et al.*, Soft Matter **6**, 1898 (2010).
[22] M. Schoen, Physica (Amsterdam) **270A**, 353 (1999).
[23] J. M. Ilnytskyi and M. R. Wilson, Comput. Phys. Commun. **148**, 43 (2002).
[24] W. Maier and A. Saupe, Z. Naturforsch. **14A**, 882 (1959).
[25] M. P. Allen, Phys. Rev. Lett. **65**, 2881 (1990).
[26] H. Löwen, Phys. Rev. E **59**, 1989 (1999).
[27] D. Guillon, P. E. Cladis, and J. Stamatoff, Phys. Rev. Lett. **41**, 1598 (1978).
[28] L. D. Landau and E. M. Lifshitz, *Statistical Physics* (Pergamon, London, 1980), Chap. 12.
[29] M. Karplus and J. N. Kushick, Macromolecules **14**, 325 (1981).
[30] F. J. Carrion *et al.*, Int. J. Mol. Sci. **10**, 4102 (2009).
[31] A. Hussain *et al.*, Biosens. Bioelectron. **25**, 1 (2009).
[32] S. Juodkazis *et al.*, J. Appl. Phys. **106**, 051101 (2009).
[33] S. H. Yang and C. S. Hsu, J. Polym. Sci. A **47**, 2713 (2009).
[34] R. Valiullin *et al.*, Phys. Chem. Chem. Phys. **11**, 2833 (2009).
[35] S. V. Dvinskikh and I. Furo, J. Chem. Phys. **115**, 1946 (2001).
[36] R. Valiullin and A. Khokhlov, Phys. Rev. E **73**, 051605 (2006).
[37] W. E. Maas *et al.*, J. Am. Chem. Soc. **118**, 13 085 (1996).
[38] E. E. Romanova *et al.*, J. Magn. Reson. **196**, 110 (2009).